Materials Today Bio 32 (2025) 101790

Contents lists available at ScienceDirect

Materials Today Bio

journal homepage: www.journals.elsevier.com/materials-today-bio

CBD-conjugated BMP-inhibiting exosomes on collagen scaffold dual-target Achilles tendon repair: Synergistic regeneration and heterotopic ossification prevention

Yan Xu [a,b,1], Jiaqiang Huang [c,1], Yingjie Mai [a,b], Zhiyuan Zhang [a,b], Siqi Li [d], Haofeng Lin [a,b], Fuxin Wei [a,b,**], Yang Chen [e,f,*]

[a] Department of Orthopaedics, The Seventh Affiliated Hospital, Sun Yat-sen University, Shenzhen, China
[b] Shenzhen Key Laboratory of Bone Tissue Repair and Translational Research, China
[c] The First District of Department of Orthopedics, Xiangtan Central Hospital, Xiangtan, China
[d] School of Public Health, Chongqing Medical University, Chongqing, China
[e] Chongqing Key Laboratory of Translational Research for Cancer Metastasis and Individualized Treatment, Chongqing University Cancer Hospital, Chongqing University, Chongqing, China
[f] Department of Thoracic Surgery, Chongqing University Cancer Hospital, Chongqing University, Chongqing, China

ARTICLE INFO

Keywords:
Achilles tendon repair
Tissue-engineered exosomes
Heterotopic ossification
BMP signaling
3D scaffold

ABSTRACT

Tendon injuries in the aging population are often complicated by heterotopic ossification (HO), hindering functional recovery. Exosomes from tendon stem/progenitor cells (TSPCs) promote regeneration but may also induce osteogenesis, contributing to HO. Preconditioning with the BMP inhibitor LDN193189 and modification with collagen-binding peptides (CBD) can enhance the tenogenic potential of exosomes while mitigating osteogenic effects. We evaluated the efficacy of a 3D-printed scaffold loaded with LDN-preconditioned, CBD-modified exosomes (3D-CBD@LDN/Exos) derived from $CD26^+$ TSPCs in promoting Achilles tendon repair and preventing HO in aged Sprague-Dawley rats. $CD26^+$ TSPCs were isolated from rat tendons, and exosomes were collected after LDN treatment and subsequently modified with CBD. A scaffold composed of PLGA and collagen I was fabricated via 3D printing and loaded with the exosomes. Rats (20 months old) with 6-mm Achilles tendon defects were randomly assigned to Control, 3D-Exos, 3D-LDN/Exos, or 3D-CBD@LDN/Exos groups, and tendon regeneration was evaluated at 4 and 12 weeks using histology, ECM quantification, micro-CT, and biomechanical testing. At 12 weeks, the 3D-CBD@LDN/Exos group exhibited near-normal histology, enhanced collagen and sGAG deposition, biomechanical properties comparable to native tendons, and significantly reduced HO, indicating that this dual-targeted strategy holds promise for tendon repair.

1. Introduction

Tendon injuries account for approximately 30 % of musculoskeletal consultations, presenting a significant challenge in both clinical and rehabilitative settings [1–4]. These injuries are particularly prevalent among physically active individuals and the aging population [5–7]. The inherently hypocellular and avascular nature of tendon tissue complicates healing, often leading to inferior biomechanical outcomes and scar tissue formation [3–5]. In some cases, this process advances to heterotopic ossification, where abnormal bone formation within the tendon further hinders recovery [2,8,9]. While conventional surgical interventions, such as tendon repair or reconstruction, can restore gross anatomical continuity, they frequently fall short in achieving full microstructural regeneration and functional restoration of the tendon, resulting in persistent pain and disability [10,11]. Therefore, there is an urgent need for more targeted therapeutic strategies that promote effective healing and reduce complications.

Recent studies have highlighted the regenerative promise of resident

This article is part of a special issue entitled: Multiscale Composites published in Materials Today Bio.

* Corresponding author. No.181, Hanyu Road, Chongqing University Cancer Hospital, Chongqing University, Chongqing, 400030, China.
** Corresponding author. No.628, Zhenyuan Road, the Seventh Affiliated Hospital, Sun Yat-sen University, Shenzhen, 518107, China.
E-mail addresses: weifuxin@mail.sysu.edu.cn (F. Wei), chenyangfighting@foxmail.com (Y. Chen).

[1] The two authors contributed equally to this paper.

https://doi.org/10.1016/j.mtbio.2025.101790
Received 24 March 2025; Received in revised form 21 April 2025; Accepted 22 April 2025
Available online 22 April 2025

tendon stem/progenitor cells (TSPCs), which can differentiate into tenocytes and contribute to extracellular matrix (ECM) deposition during healing [12–14]. However, the inflammatory microenvironment of injured tendon often misdirects TSPC fate toward chondrogenic or osteogenic lineages, exacerbating HO and fibrosis [15,16]. A distinct subset of $CD26^+$ TSPCs located in the peritendon exhibits enhanced tenogenic potential but also drives ectopic ossification under dysregulated BMP signaling [17,18]. Thus, strategies are needed to harness $CD26^+$ TSPCs' regenerative capacity while mitigating their osteogenic tendencies.

Heterotopic ossification, a pathological process marked by bone formation within soft tissues, is largely regulated by the bone morphogenetic protein (BMP) signaling pathway [8,19,20]. Growth factor-loaded scaffolds (e.g., TGF-β1, BMP-12, PDGF) have shown promise for enhancing tenogenic differentiation and ECM synthesis, but they do not address the risk of aberrant osteogenesis within the injured tendon [5,21]. LDN193189 (LDN), a BMP receptor inhibitor, specifically targets activin receptor-like kinases 2 (ALK2) and ALK3 [22]. The high specificity of LDN for BMP receptors helps prevent osteogenesis and adipogenesis, reducing heterotopic ossification formation [23]. Here, early intervention with LDN or similar BMP inhibitors in $CD26^+$ TSPCs might preserve their tenogenic potential while preventing osteogenic differentiation, thus enhancing functional recovery in tendon injuries.

Exosome-based therapies derived from stem cells offer an alternative to traditional stem cell treatments, with benefits such as low immunogenicity, stability, and the absence of tumorigenic risk [24–26]. More recent efforts have employed exosome-loaded scaffolds to harness the pro-regenerative paracrine functions of stem cell–derived vesicles; however, these platforms generally lack mechanisms to suppress exosomal osteogenic cargo, leading to uncontrolled bone formation in some contexts [27,28]. Additionally, the passive diffusion of unmodified exosomes from conventional scaffolds leads to rapid clearance and limited retention at the injury site, thereby diminishing the duration and efficacy of tenogenic signaling. To address these challenges, we utilized exosomes derived from $CD26^+$ TSPCs, preconditioned with the BMP inhibitor LDN and integrated into a bioengineered scaffold.

Collagen, a major ECM component, is known for its biocompatibility, low immunogenicity, and cell adhesion properties, making it an ideal material for promoting tenogenic differentiation [5,24,29]. The collagen-binding domain (CBD), a polypeptide consisting of TKK- TLRT amino acids, derived from collagenase, binds specifically to collagen I-based biomaterials and has shown promise in targeting injured tissues for drug delivery, including in spinal cord injury treatment [30,31]. Poly (d, l-lactic-co-glycolic acid) (PLGA), an FDA-approved biomaterial, is commonly used in tissue regeneration due to its favorable mechanical properties and biocompatibility [32,33]. Recent advances in 3D bioprinting allow the creation of scaffolds that integrate bioactive factors while maintaining their efficacy, and can be designed to facilitate cell infiltration and tissue regeneration [24,34]. The combination of these materials yields a biomimetic scaffold that closely replicates the native tendon environment and enables controlled, sustained release of exosomes.

In this study, we aim to develop a novel scaffold composed of LDN-preconditioned, CBD-decorated exosomes derived from $CD26^+$ TSPCs, loaded onto a collagen I/PLGA matrix using 3D bioprinting (3D-CBD@LDN/Exos). This scaffold will be designed to target tendon regeneration while preventing heterotopic ossification formation. We will assess the impact of scaffold on cellular activity in vitro and evaluate its efficacy in a rat model of Achilles tendon injury. This approach has the potential to significantly improve tendon healing outcomes and mitigate the long-term consequences of heterotopic ossification.

2. Materials and methods

2.1. Ethics statement

The experimental protocol (SYSU-IACUC-2024-001252) was approved by the local animal ethics committee for the use of Sprague-Dawley (SD) rats. To ensure both scientific validity and ethical compliance, the required rat sample size for evaluating tendon healing was determined through rigorous statistical power analyses. These analyses, guided by established standards, were performed with an effect size of 70 %, $\alpha = 00.05$, and power of 0.80, maintaining a balance between research rigor and animal welfare considerations.

2.2. $CD26^+$ TSPCs isolation and culture

Primary tendon-derived cells were isolated from the Achilles tendons of 6-week-old SD rats. Tendon sheaths were removed, and tendons were minced and digested with collagenase I (1.5 mg/mL, MilliporeSigma) and dispase (2 mg/mL, Roche) at 37 °C for 30 min. The digestion solution was centrifuged (500g, 5 min), supernatant discarded, and the precipitate washed with FACS buffer. Flow cytometry was used to analyze surface markers: FITC-CD45 (Biolegend, 202205), FITC-Ter119 (Invitrogen, MA5-17580), FITC-CD31 (Invitrogen, MA5-16952), APC/Cyanine7-CD90 (Biolegend, 202519), APC-CD73 (Bioss, bs-4834R-APC), and PE-CD26. $CD26^+$ TSPCs (Invitrogen, MA5-17551) were sorted using a Beckman Coulter XL System and analyzed with FlowJo 10. Fluorescence-activated cell sorting was performed on a BD FACSAria II system configured with a 100 μm nozzle and 20 psi sheath pressure in high-purity mode. Cells were gated sequentially for live singlets (FSC-A/SSC-A, DAPI−), lineage exclusion (CD31/Ter119/CD45 triple-negative, thresholds at 99th percentile via isotype controls), and positive selection (CD90/CD73/CD26 triple-positive, thresholds defined by fluorescence-minus-one controls). Daily compensation calibration using UltraComp eBeads ensured spectral accuracy. Post-sort reanalysis (FlowJo v10.8.1) confirmed >95 % purity of $CD26^+$ TSPCs, which were cultured in DMEM/low glucose supplemented with 10 % FBS under standard conditions (37 °C, 5 % CO_2), with strict passage limitation to maintain progenitor potency. All reagents, antibody clones, and instrument parameters were fully documented to ensure experimental reproducibility.

2.3. Stable cell line construction

The gcGFP-CBD-tag-Lamp2b expression vector was designed and purchased from Genechem Co., Ltd. (Shanghai, China). Lentiviral transduction of $CD26^+$ TSPCs was performed per manufacturer instructions, and puromycin selection was used to obtain purified RGD-TSPCs.

2.4. Exosome isolation and characterization

$CD26^+$ TSPCs were treated with LDN (1 μM) for 24 h (Fig. 1A), followed by culture in exosome-free medium for 48 h. Conditioned media were collected, centrifuged (10,000g, 30 min; 100,000g, 70 min, 4 °C), and the pellets resuspended in PBS. Three exosome groups were prepared: untreated (Exos), LDN-treated (LDN/Exos), and RGD-TSPC-derived LDN-treated (CBD@LDN/Exos). Exosome morphology was examined via transmission electron microscopy (TEM), size was determined by nanoparticle tracking analysis (NTA), and protein content was quantified using a BCA assay. Western blotting was performed to assess exosomal markers CD9, CD63, Lamp2b, and TSG101.

2.5. Effects of LDN-Exos on cultured BMSCs

Rat bone marrow mesenchymal stem cells (BMSCs, RASMX-01001; Cyagen, China) at passage 3 were seeded in 48-well plates at 1.5×10^4 cells/cm^2 in α-MEM for 24 h, then treated with Exos or LDN/Exos

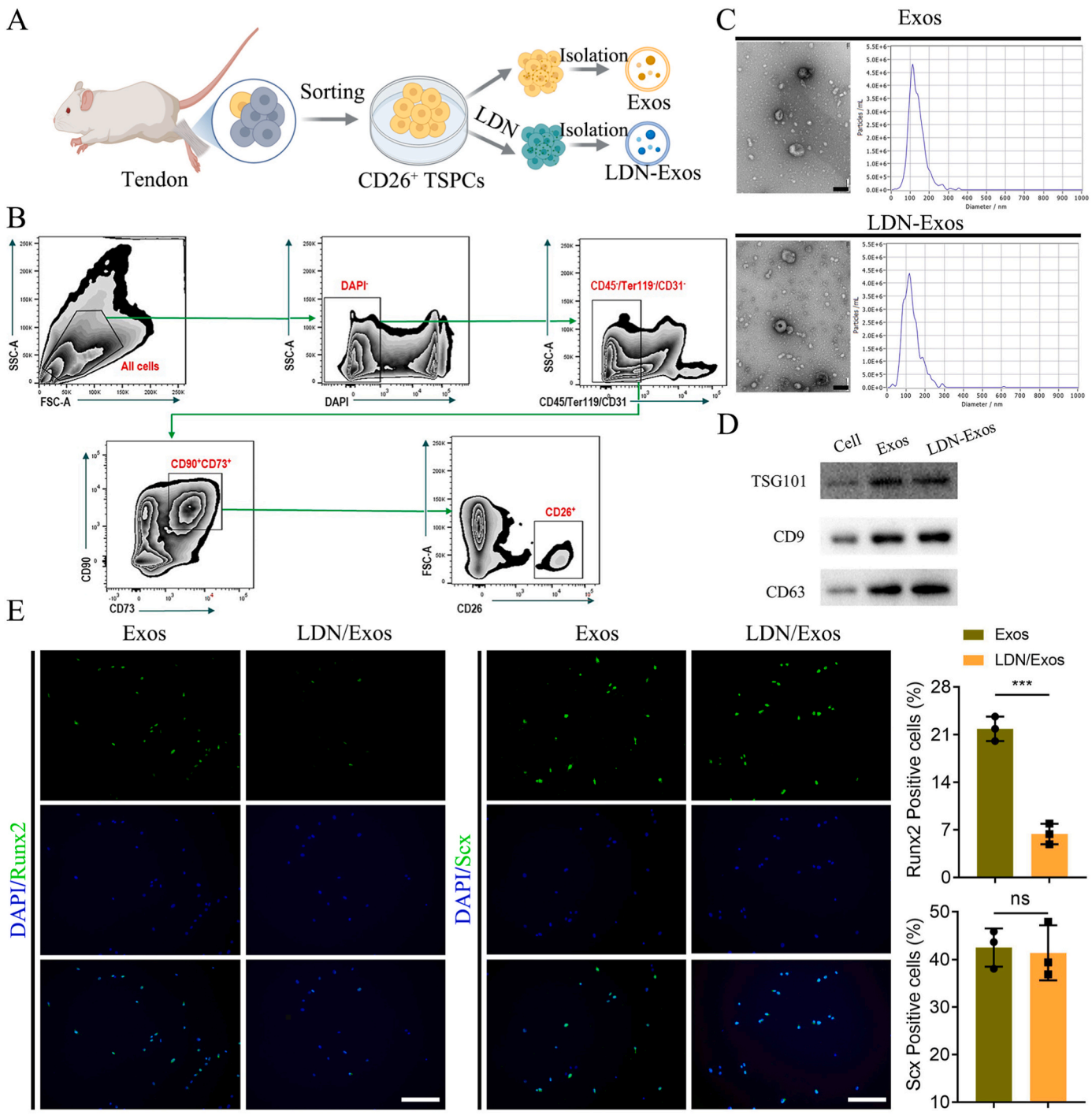

Fig. 1. Characterization of exosomes derived from CD26$^+$ TSPCs and those preconditioned with LDN. (A) The schematic workflow for the extraction of Exos and LDN/Exos. (B) Representative flow cytometry plots used to isolate CD26$^+$ TSPCs, highlighting positive markers CD26, CD90, and CD73, and negative markers Ter119, CD31, and CD45. (C) Transmission electron microscopy images and nanoparticle tracking analysis of Exos and LDN/Exos. Scale bar = 100 nm. (D) Western blot analysis of exosomal markers, including CD9, CD63, and TSG101. (E) Immunofluorescence images of Scx and Runx2 expression in BMSCs treated for 7 days with Exos or LDN/Exos. Scale bar = 200 μm. Data are expressed as mean ± standard deviation ("ns" $P > 0.05$, "***" $P < 0.001$).

(50 ng/mL) in α-MEM supplemented with 1 % FBS. After 7 days, immunofluorescence staining for scleraxis (Scx, ab58655; Abcam) and Runt-related transcription factor 2 (Runx2, 20700-1-AP; Proteintech) was performed to evaluate tenogenic and osteogenic induction.

2.6. 3D-printed scaffold fabrication and characterization

Preparation of Low-Temperature Rapid 3D-Printed Exos/PLGA/Col I Scaffolds: At room temperature, PLGA was dissolved in 1,4-dioxane under magnetic stirring for 30 min to yield a homogeneous polymer solution suitable for low-temperature phase separation. Lyophilized exosomes (1×10^{11} particles/mL) and type I collagen were gently incorporated and stirred for 10 min, ensuring even dispersion of vesicles without compromising their integrity. The resulting bio-ink was printed on an ultra-low-temperature platform via a 300 μm nozzle at 5–10 mm/s, producing scaffolds with designed filament diameters (~300 μm) and interconnected pores (~500 μm) using LDM technology. These included exosomes derived from CD26$^+$ TSPCs (3D-Exos), LDN-treated exosomes

(3D-LDN/Exos), and CBD-modified LDN-treated exosomes (3D-CBD@LDN/Exos). The fabricated 3D-printed scaffolds were lyophilized using a vacuum freeze-dryer (FD8-5T, SIM, Newark, NJ, USA). Subsequently, scaffold characterization was performed via scanning electron microscopy (SEM; S-3400 N, Hitachi, Japan) for microstructure analysis, ethanol replacement for porosity determination, and an Instron testing system for mechanical property evaluation.

2.7. Scaffold cytotoxicity and biocompatibility

BMSCs were seeded onto 3D-LDN/Exos and 3D-CBD@LDN/Exos scaffolds at 2×10^4 cells/cm^2. After 3 days, cell viability was assessed using calcein-AM/propidium iodide staining, and the percentage of live cells was calculated.

2.8. Tenogenic and osteogenic potential of scaffolds

BMSCs were seeded onto scaffolds and TCPS (control) at 1.5×10^4 cells/cm^2, cultured for 7 days, and then analyzed via immunofluorescence for Scx and Runx2 expression.

2.9. Exosome release kinetics

Scaffolds were incubated in PBS at 37 °C, with supernatants collected at days 0, 1, 3, 7, 14, and 21; after each collection, fresh PBS was added. Exosomal protein concentrations in the supernatants were measured using a BCA assay. Additionally, a 3D scaffold without exosomes was used as a substrate control to account for protein degradation effects.

2.10. In vivo tracking of DiR-Labeled exosomes

Exosomes were labeled with DiR dye, washed, and collected. Labeled 3D-LDN/Exos and 3D-CBD@LDN/Exos scaffolds were implanted into tendon defects, and fluorescence intensity was monitored using an IVIS Spectrum imaging system.

2.11. Animal model and surgical procedure

A total of 112 male 20-month-old SD rats were randomly assigned to four groups (n = 14 per group per time point): Control (untreated Achilles tendon defect), 3D-Exos, 3D-LDN/Exos, and 3D-CBD@LDN/Exos. Rats were sacrificed at postoperative weeks 4 or 12 for Achilles tendon specimen collection. At each time point, six specimens per group were used for micro-CT and histological evaluations, and the remaining eight were used for biomechanical testing.

A 6-mm defect was created in the midsubstance of the Achilles tendon as previously described [5]. Under anesthesia with 3 % pentobarbital sodium (0.8 mL/kg, i.v.), a midline incision was made 3 mm distal to the gastrocnemius muscle and 3 mm proximal to the calcaneus to expose the tendon complex. A 6-mm defect involving both the medial and lateral gastrocnemius was generated. Immediately following tenotomy, the defect was bridged with the appropriately shaped scaffold (3D-Exos, 3D-LDN/Exos, or 3D-CBD@LDN/Exos) using a modified Kessler suture technique with 6-0 PDS absorbable sutures (Ethicon Inc., Johnson & Johnson, New Jersey, USA). The paratenon was closed with 6-0 PDS sutures, and the skin was approximated with nonabsorbable Monosof 3-0 sutures (Medtronic, Milan, Italy).

To enhance heterotopic ossification, in addition to using elderly rats (≥18 months old), the calcaneal periosteum was thoroughly scraped during surgery [19,35,36]. Postoperatively, tramadol (Grunenthal GmbH) was administered on days 1–3, and rats were allowed unrestricted cage activity. All procedures were performed under sterile conditions by experienced surgeons.

2.12. Micro-CT analysis

Hindlimbs (n = 6 per group at each time point) were fixed in 4 % paraformaldehyde and scanned using a μCT 80 system (Switzerland) at 80 kV and 20 μm resolution per pixel. Regions of heterotopic ossification in the Achilles tendon were reconstructed to quantify bone volume and density.

2.13. Histological evaluation

AT specimens (n = 6 per group at each time point), fixed in 4 % paraformaldehyde for 12 h, were dehydrated, paraffin-embedded, and sectioned coronally at 5 μm. Sections were stained with H&E, Masson's Trichrome (MT), and Picrosirius Red (PR) to assess neo-tendon formation. Collagen I and III expressions were evaluated via immunohistochemistry (anti-collagen I, ab6308, Abcam; anti-collagen III, ab23445, Abcam). Two blinded observers scored the tissue using the modified Mankin's system, grading fiber structure, arrangement, nuclear rounding, vascularity, inflammation, and cellularity on a 0–3 scale (Table S1).

2.14. Collagen and sulfated glycosaminoglycan (sGAG) content

Native and regenerated tendon samples (n = 6 per group at each time point) were minced (~1 mm^3) and digested with pepsin (1 mg/mL in 0.5 M acetic acid). Collagen content was determined using a Sircol Collagen Assay (S1000; Biocolor) following the manufacturer's instructions. For sGAG quantification, the same digested supernatants were assayed using dimethylmethylene blue (DMMB); 16 mg DMMB was dissolved in 1 L of water containing 3.04 g glycine, 2.37 g NaCl, and 95 mL 0.1 M HCl. Five microliters of each sample was mixed with 200 μL DMMB solution, and absorbance was measured at 525 nm. A calibration curve prepared with chondroitin sulfate enabled sGAG quantification.

2.15. Tensile testing

AT specimens (n = 8 per group at each time point) were mounted on an Instron Tension System (Instron, USA) using a sandpaper-assisted upper clamp for the tendon and a lower clamp for the calcaneus (Fig. 7A). Thickness and width were measured three times under a 0.1-N preload to calculate the cross-sectional area (CSA). Following a 0.1-N preload for alignment, samples were loaded to failure at 10 mm/min. The failure load was recorded from the load-displacement curve and normalized to the CSA to compute ultimate stress (MPa). Specimens were kept moist with 0.9 % saline during testing.

2.16. Statistical analysis

Sample sizes were determined by power analysis. Data were analyzed using SPSS 25.0, with results expressed as mean ± SD. One-way ANOVA with post hoc tests assessed differences among groups, while Mann-Whitney tests analyzed histological scores. Significance was set at $P < 0.05$.

3. Results

3.1. Identification and characterization of CD26$^+$ TSPCs and their exosomal secretions

We isolated CD26$^+$ TSPCs from rat tendon tissues, identifying them by positive expression of CD26, CD90, and CD73, and negative expression of hematopoietic markers CD45, Ter119, and CD31 (Fig. 1B). Transmission electron microscopy (TEM) revealed that exosomes derived from these cells (Exos) exhibited a typical double-layered, cup-shaped morphology, predominantly ranging from 100 to 200 nm in size, as confirmed by nanoparticle tracking analysis (NTA) (Fig. 1C). Western blot analysis detected high levels of exosomal markers, including CD9,

CD63, and TSG101 (Fig. 1D). To assess the functional impact of exosomes, BMSCs were treated with Exos or LDN-preconditioned exosomes (LDN/Exos). Immunofluorescence assays (Fig. 1E) demonstrated that LDN/Exos maintained the tenogenic differentiation potential of Exos while reducing their osteogenic effects, suggesting that LDN/Exos are promising candidates for promoting tendon regeneration without inducing heterotopic ossification.

3.2. 3D-printed scaffold exhibits excellent physical properties and biocompatibility

The 3D-CBD@LDN/Exos scaffold was fabricated via 3D printing using a collagen I/PLGA composite (Fig. 2A). Western blot analysis confirmed that Lamp2b expression was higher in CBD@LDN/Exos than in LDN/Exos, verifying effective decoration of exosomes with CBD peptides (Fig. 2B). SEM revealed a porous structure in the 3D-CBD@LDN/Exos scaffold, providing an optimal environment for cell attachment and proliferation (Fig. 2C). Mechanical testing showed no significant differences in tensile stress or porosity among scaffolds

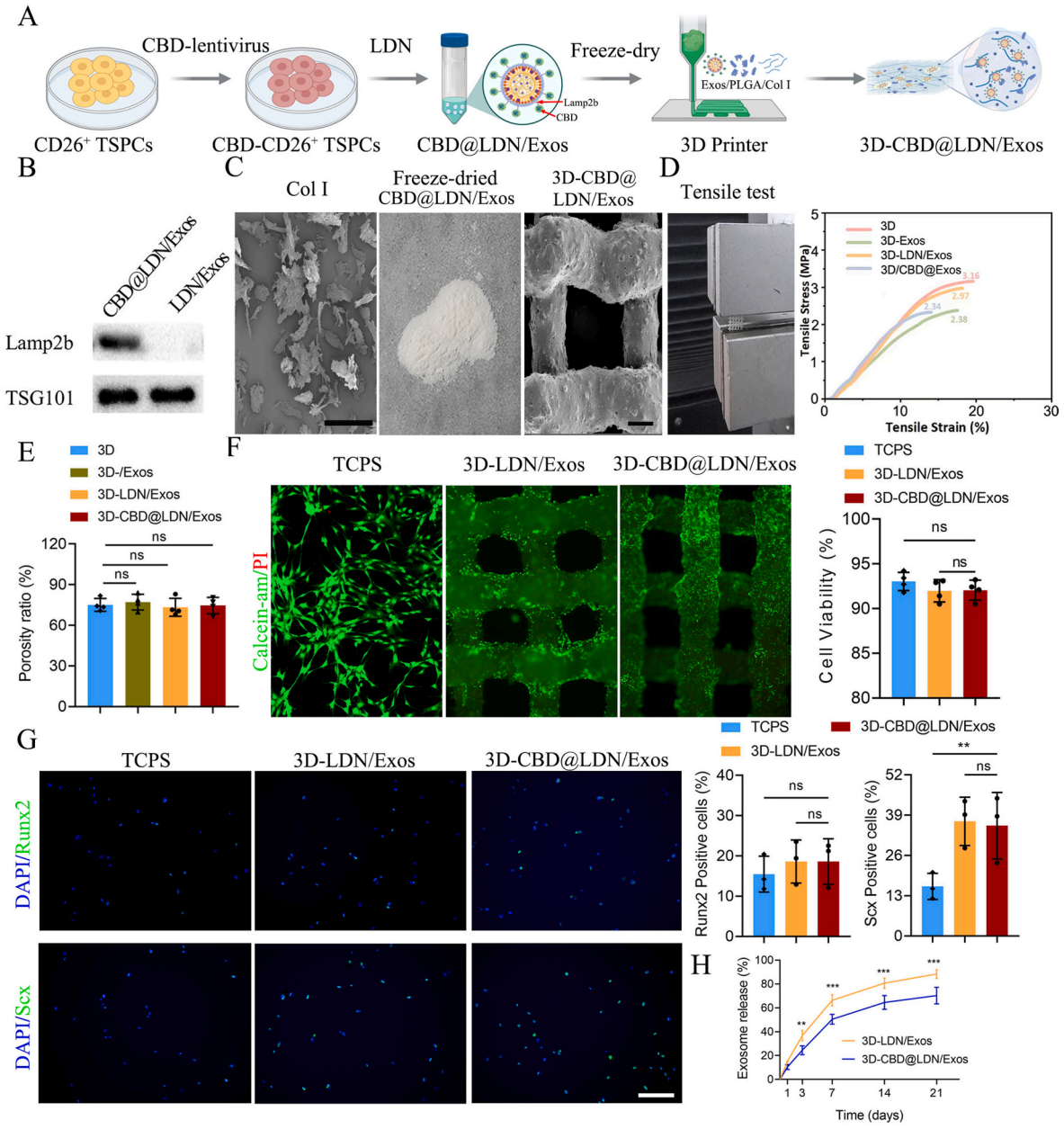

Fig. 2. Preparation and characterization of the 3D-CBD@LDN/Exos. (A) Schematic diagram of the fabrication process for 3D-CBD@LDN/Exos. (B) Western blot analysis showing Lamp2b expression in LDN/Exos versus CBD@LDN/Exos. (C) SEM images of type I collagen, freeze-dried exosome powder, and the final scaffold. Scale bar = 200 μm. (D) Diagram illustrating scaffold stretching and corresponding tensile stress measurements. (E) Porosity ratios of the scaffolds. (F) Live/dead assay of BMSCs seeded for 3 days on TCPs, 3D-LDN/Exos, and 3D-CBD@LDN/Exos; representative images display live (green) and dead (red) cells, with quantitative viability analysis. (G) Immunofluorescence images showing Scx and Runx2 expression in BMSCs after 7 days of co-culture on TCPs, 3D-LDN/Exos, and 3D-CBD@LDN/Exos. Scale bar = 200 μm. (H) Cumulative release profiles of exosomes from 3D-LDN/Exos and 3D-CBD@LDN/Exos over 21 days. Data are presented as mean ± standard deviation ("ns" $P > 0.05$, "**" $P < 0.01$, "***" $P < 0.001$). (For interpretation of the references to color in this figure legend, the reader is referred to the Web version of this article.)

loaded with different exosomes, indicating that the incorporation of PLGA and collagen I maintained consistent physical properties (Fig. 2D and E). Live/Dead assays demonstrated high cell viability of BMSCs on both 3D-CBD@LDN/Exos and 3D-LDN/Exos scaffolds, with cytotoxicity levels comparable to those observed on TCPS (Fig. 2F).

3.3. Tenogenic and osteogenic inducibility and sustained Exosome release

Immunofluorescence analysis revealed that both 3D-CBD@LDN/Exos and 3D-LDN/Exos scaffolds promoted tenogenic differentiation of BMSCs, as indicated by enhanced Scx expression compared to the TCPS control (Fig. 2G). In contrast, Runx2 expression, a marker of osteogenesis, showed no significant differences between the two scaffold groups, suggesting that CBD modification does not alter the exosomes' biological effects on osteogenesis. Release kinetics studies further demonstrated distinct exosome release profiles: while 3D-LDN/Exos exhibited a burst release pattern, 3D-CBD@LDN/Exos released exosomes in a sustained manner. After 21 days in PBS, only 9.59 ± 3.14 % of exosomes remained in 3D-LDN/Exos compared to 29.71 ± 6.90 % in 3D-CBD@LDN/Exos ($P < 0.001$) (Fig. 2H). These findings suggest that the 3D-CBD@LDN/Exos scaffold not only provides structural support for tendon regeneration but also serves as an efficient delivery system for sustained exosome release at the AT defect site.

3.4. Sustained in vivo release of exosomes from the 3D-CBD@LDN/Exos Scaffold

Fig. 3 illustrates the in vivo tracking of DiR-labeled exosomes delivered via scaffolds implanted at tendon defect sites. Both 3D-LDN/Exos and 3D-CBD@LDN/Exos scaffolds were used, and the IVIS Imaging System captured their spatiotemporal distribution. Notably, red fluorescence persisted at the injury site for up to 21 days in the 3D-CBD@LDN/Exos group, indicating a sustained release of exosomes compared with the 3D-LDN/Exos scaffold.

3.5. 3D-CBD@LDN/Exos Scaffold effectively prevented tendon heterotopic ossification

Fig. 4A shows that micro-CT analysis at 4 and 12 weeks post-surgery revealed significant differences in heterotopic ossification among the groups. Specifically, the 3D-CBD@LDN/Exos group exhibited lower heterotopic ossification volume and density than both the control and 3D-Exos groups at 4 and 12 weeks. Although there was no significant difference between the 3D-CBD@LDN/Exos and 3D-LDN/Exos groups at 4 weeks, by 12 weeks the 3D-CBD@LDN/Exos group demonstrated a marked reduction in heterotopic ossification compared with the 3D-LDN/Exos group (Fig. 4B). These results indicate that the 3D scaffold loaded with exosomes preconditioned with LDN and modified with CBD effectively suppresses tendon heterotopic ossification.

3.6. Histological observation

Due to the use of aged rats and extensive calcaneal periosteum removal, the control group exhibited disorganized collagen, abundant round nuclei, and pronounced heterotopic ossification. At 4 weeks post-surgery (Fig. 5A), the 3D-Exos group showed only minor histological

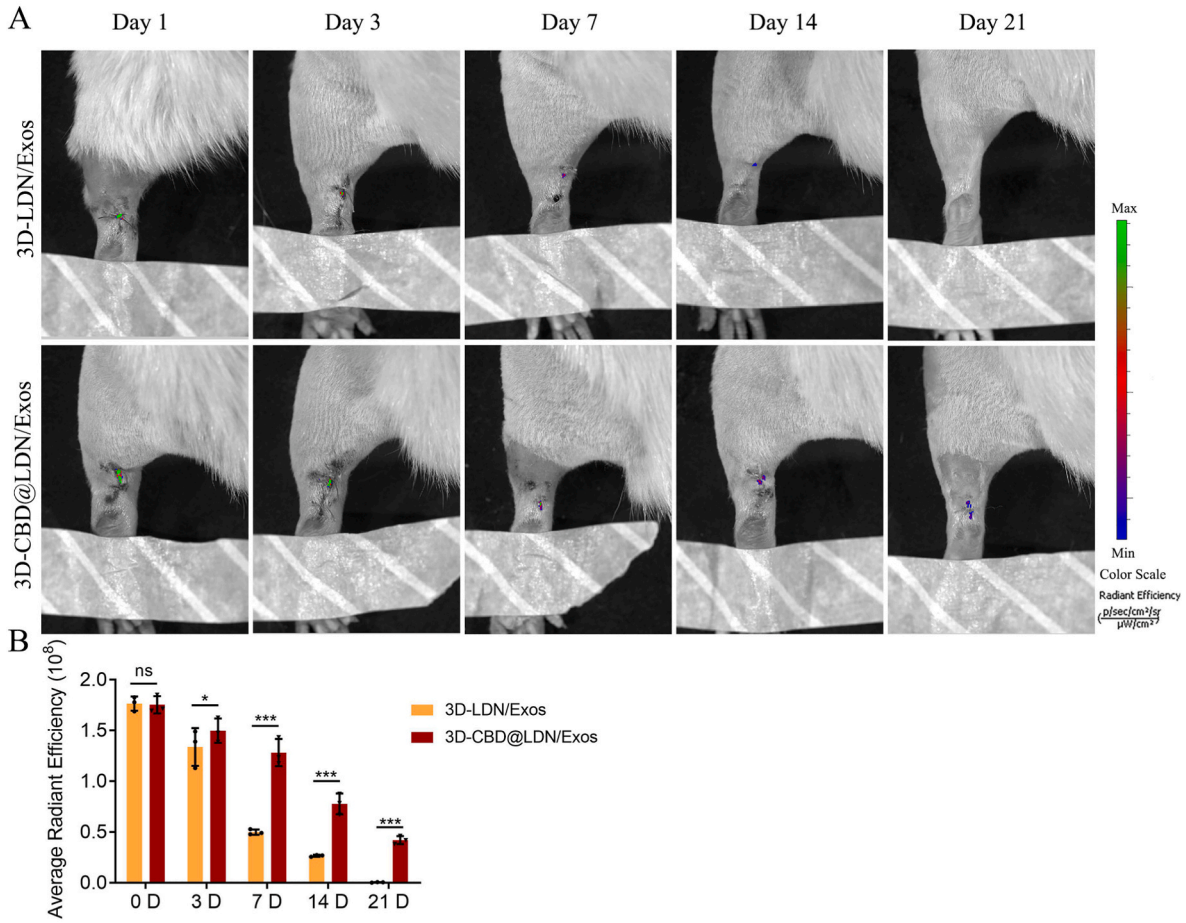

Fig. 3. In vivo exosome release from the 3D-CBD@LDN/Exos Scaffold. (A) In vivo imaging of DiR-labeled exosomes delivered via scaffolds implanted at tendon defect sites, demonstrating sustained release. (B) Semi-quantitative analysis of average radiant efficiency over time. Data are expressed as mean ± standard deviation ("ns" $P > 0.05$, "*" $P < 0.05$, "***" $P < 0.001$).

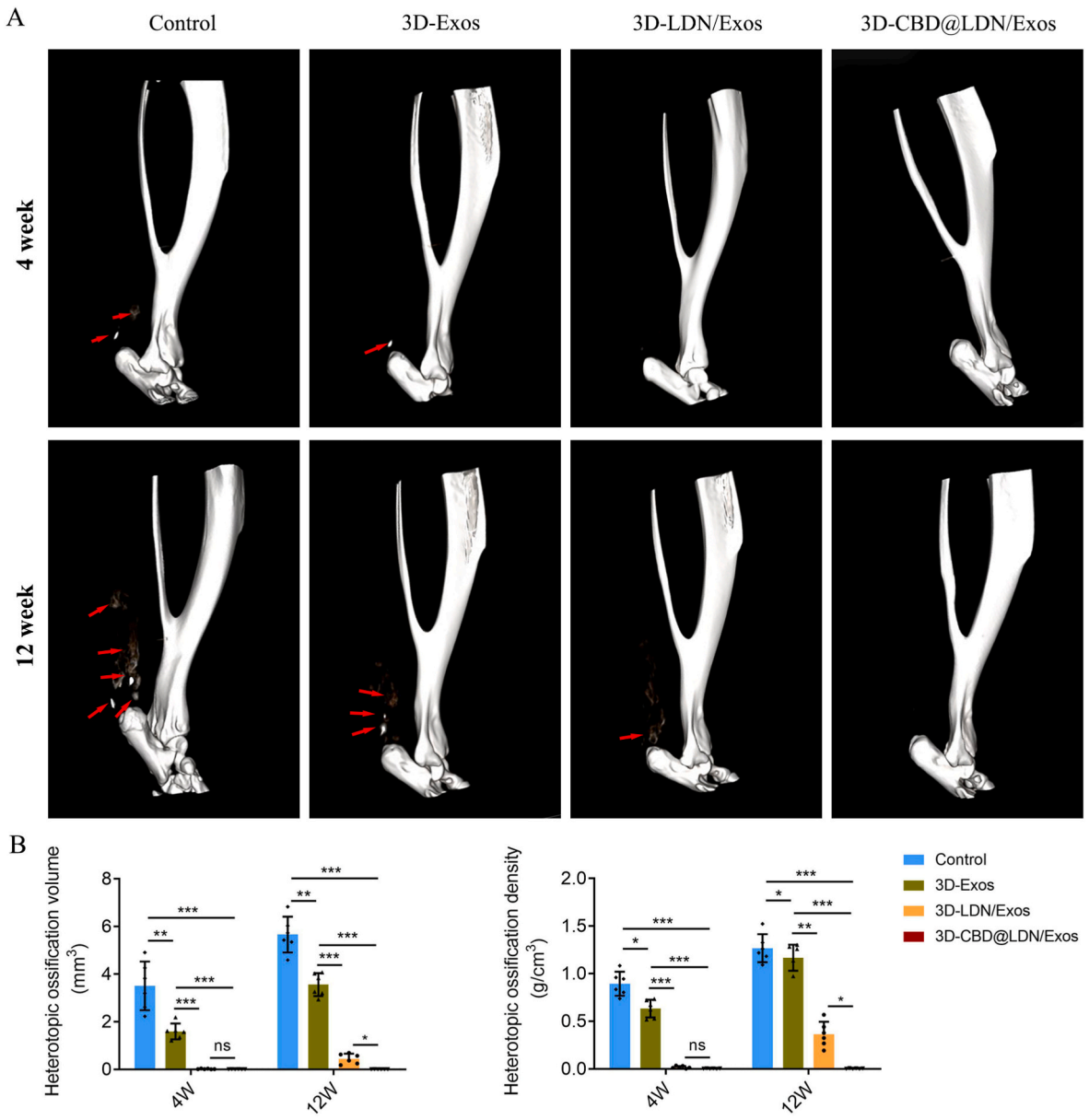

Fig. 4. Imaging evaluation of heterotopic ossification. (A) Representative micro-CT images of heterotopic ossification in rat Achilles tendons at 4 and 12 weeks postoperatively. (B) Quantitative analysis of heterotopic ossification volume and density across the four groups. Data are expressed as mean ± standard deviation ("ns" $P > 0.05$, "*" $P < 0.05$, "**" $P < 0.01$, "***" $P < 0.001$).

improvements, whereas both the 3D-LDN/Exos and 3D-CBD@LDN/Exos groups demonstrated significant amelioration of tendon architecture. By 12 weeks, all scaffold implants were completely internalized and absorbed. Notably, the 3D-CBD@LDN/Exos group exhibited a nearly normal histologic appearance—with spindle-shaped fibroblasts embedded in a matrix of parallel fibers—confirmed by H&E, MT, and PR staining.

Modified Mankin's scoring (Fig. 5B) revealed that the neo-tendon in the 3D-CBD@LDN/Exos group had significantly lower histological scores than those in the control and 3D-Exos groups. Although there was no significant difference between the 3D-LDN/Exos and 3D-CBD@LDN/Exos groups at 4 weeks, the 3D-CBD@LDN/Exos group showed a significantly lower score than the 3D-LDN/Exos group at 12 weeks ($P < 0.05$). These results indicate that scaffolds loaded with LDN-preconditioned exosomes markedly promote tendon regeneration compared to controls and 3D-Exos scaffolds, and that CBD modification further enhances long-term regenerative outcomes. Additionally, the porous, loose structure of the 3D-CBD@LDN/Exos scaffold appears more conducive to tendon healing while concurrently suppressing heterotopic ossification.

3.7. Immunohistochemical and Collagen/sGAG content examination

Immunohistochemical analysis (Fig. 6A) was used to evaluate the expression of Collagen I and Collagen III in neo-tendons. At 4 weeks postoperatively, the 3D-LDN/Exos and 3D-CBD@LDN/Exos groups exhibited slightly higher Collagen I expression compared to the control and 3D-Exos groups, while Collagen III expression did not differ significantly among the groups. At 12 weeks, both the 3D-LDN/Exos and 3D-CBD@LDN/Exos groups maintained higher levels of Collagen I and Collagen III relative to the control and 3D-Exos groups; notably, the 3D-CBD@LDN/Exos group demonstrated especially well-organized fiber alignment.

Collagen and sGAG content were quantified (Fig. 6B). At 4 weeks, no

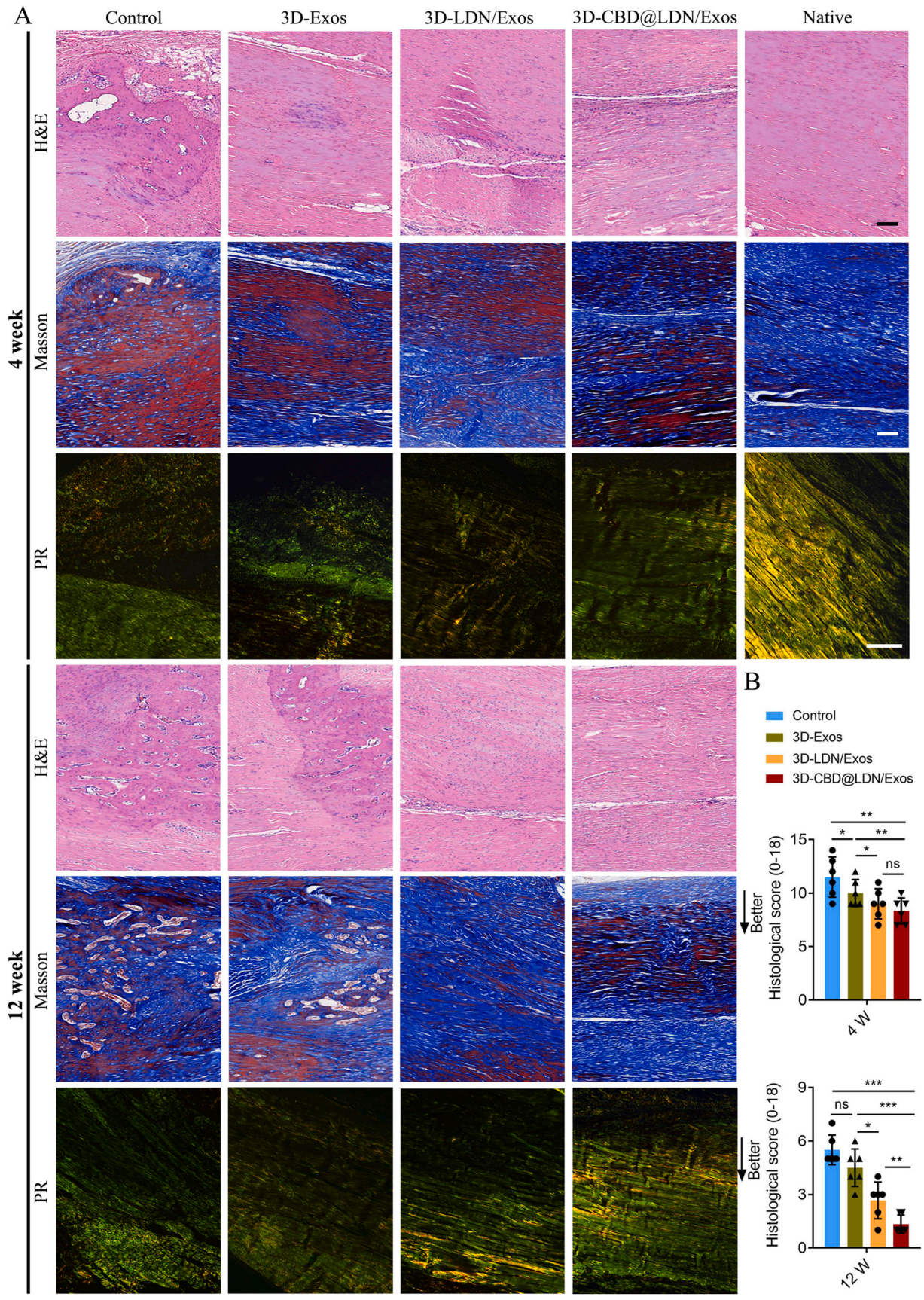

Fig. 5. Histological Analysis of Regenerated Achilles Tendon. (A) Representative images of AT sections stained with H&E, MT, and PR at 4 and 12 weeks post-operatively, with AT from a healthy rat serving as the native control. Scale bar = 100 μm. (B) Comparison of histological scores for regenerated AT among the control, 3D-Exos, 3D-LDN/Exos, and 3D-CBD@LDN/Exos groups. Data are expressed as mean ± standard deviation. ("ns" $P > 0.05$, "*" $P < 0.05$, "**" $P < 0.01$, "***" $P < 0.001$).

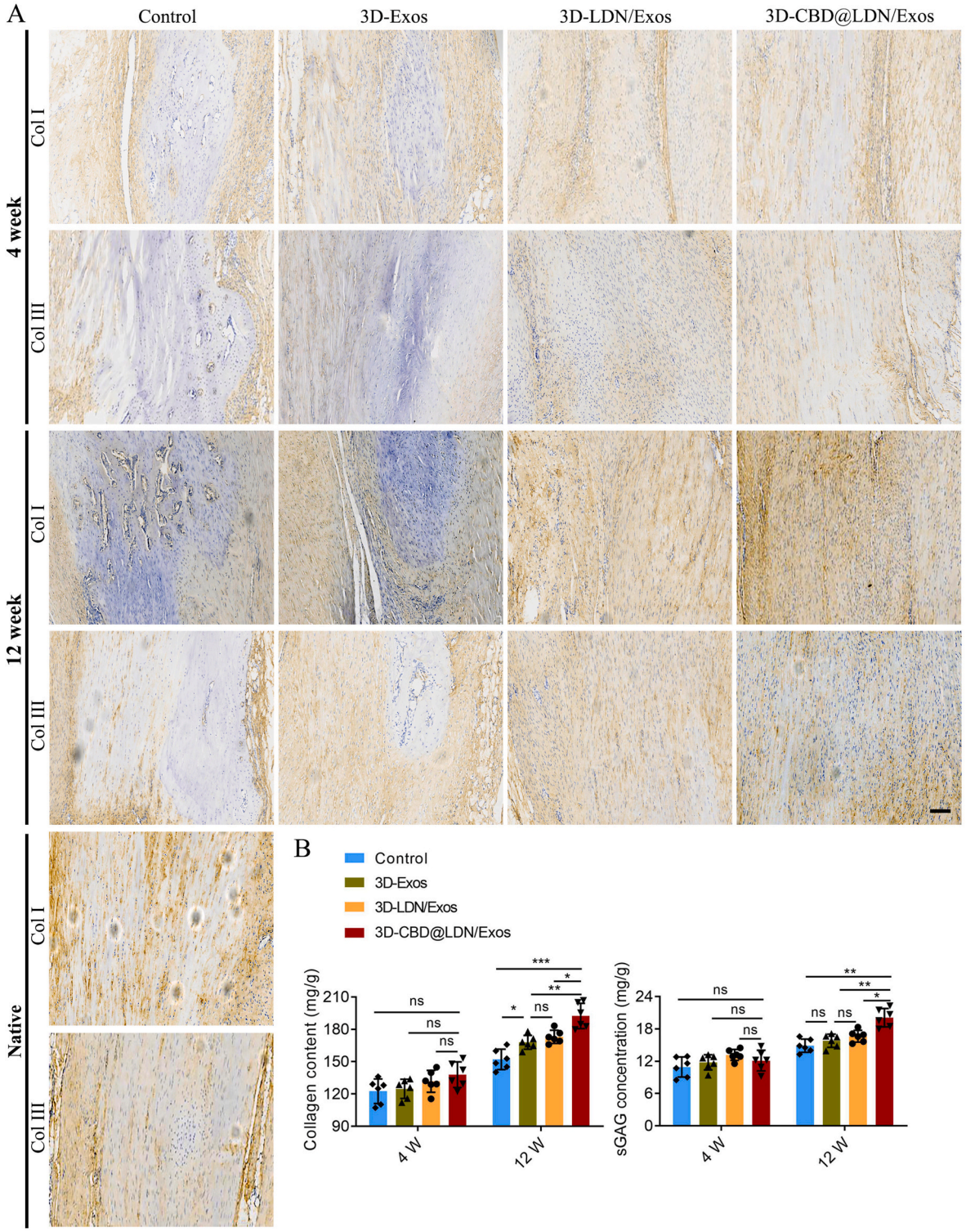

Fig. 6. Immunohistochemical analysis and ECM quantification in regenerated Achilles tendons at 4 and 12 weeks post-surgery. (A) Representative images showing Collagen I and Collagen III immunostaining. Scale bar = 100 μm. (B) Quantitative assays of collagen and sulfated glycosaminoglycans (sGAG) deposition across experimental groups. Data are presented as mean ± standard deviation. ("ns" $P > 0.05$, "*" $P < 0.05$, "**" $P < 0.01$, "***" $P < 0.001$).

significant differences were observed among the groups; however, by 12 weeks, the 3D-CBD@LDN/Exos group exhibited significantly greater collagen and sGAG deposition than the other groups. These results indicate that scaffolds loaded with LDN-preconditioned exosomes enhance extracellular matrix synthesis over time, and that CBD modification further improves fiber organization and extracellular matrix (ECM) quality, thereby supporting superior tendon regeneration.

3.8. Tensile properties of repaired Achilles tendons

At 4 weeks post-surgery, the failure load and ultimate stress in the control, 3D-Exos, 3D-LDN/Exos, and 3D-CBD@LDN/Exos groups were significantly lower than those in native tendons ($P < 0.05$ for all), with no significant differences among the experimental groups (Fig. 7B). By 12 weeks, the control, 3D-Exos, and 3D-LDN/Exos groups continued to

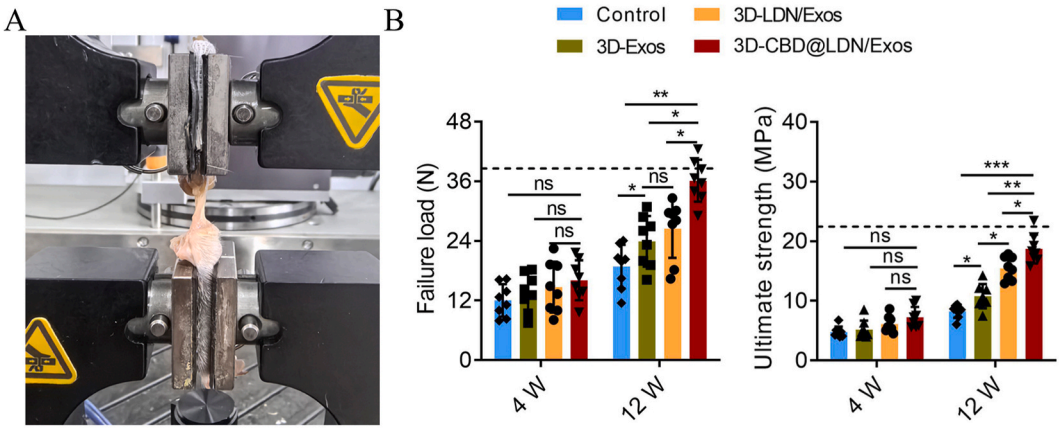

Fig. 7. Biomechanical testing of regenerated Achilles tendons at 4 and 12 weeks post-surgery. (A) Schematic representation of the mounting setup: the upper clamp (with sandpaper) secures the tendon, and the lower clamp grips the calcaneus. (B) Failure load and ultimate stress values for each experimental group; the black dotted line represents the mean values for native Achilles tendons. Data are presented as mean ± standard deviation. ("ns" $P > 0.05$, "*" $P < 0.05$, "**" $P < 0.01$, "***" $P < 0.001$).

show lower mechanical properties compared with native tendons (failure load: 38.57 ± 3.32 N; ultimate stress: 22.47 ± 1.85 MPa), whereas the 3D-CBD@LDN/Exos group reached levels comparable to native tissue. Additionally, both the 3D-Exos and 3D-LDN/Exos groups exhibited significantly higher failure load and ultimate stress than the control group, demonstrating that exosome-loaded scaffolds enhance mechanical recovery of AT defects. Notably, the 3D-CBD@LDN/Exos group showed significantly higher mechanical properties than the 3D-LDN/Exos group, indicating that CBD modification further improves the efficacy of LDN-preconditioned exosomes in promoting tendon healing. All specimens ruptured at the regenerated AT site during biomechanical testing, and no specimens were excluded.

4. Discussions

Our study provides compelling evidence that a 3D scaffold loaded with LDN-preconditioned, CBD-modified exosomes (3D-CBD@LDN/Exos) derived from $CD26^{+}$ tendon stem/progenitor cells markedly enhances Achilles tendon regeneration while concurrently suppressing heterotopic ossification. Compared with control and other exosome-loaded scaffolds, the 3D-CBD@LDN/Exos scaffold achieved superior extracellular matrix (ECM) deposition, improved fiber organization, and better mechanical recovery, as demonstrated by histological analysis, ECM quantification, and biomechanical testing.

A key innovation in our approach is the therapeutic use of exosomes. These nanoscale vesicles are rich in proteins, microRNAs, and other signaling molecules that can modulate cellular behavior [37,38]. In tendon repair, exosomes derived from TSPCs have been shown to promote tenogenic differentiation and stimulate ECM synthesis, both of which are critical for effective healing [39,40]. LDN193189 is a potent, selective inhibitor of BMP type I receptors ALK2 and ALK3, which prevents phosphorylation and nuclear translocation of Smad1/5/8, thereby blocking osteogenic transcriptional programs (RUNX2, ALP, OCN) and shifting cellular responses away from aberrant bone formation [41]. Our findings further reveal that exosomes preconditioned with the BMP inhibitor LDN193189 retain their capacity to stimulate tenogenesis while mitigating osteogenic differentiation. Heterotopic ossification is a significant clinical challenge in tendon repair, often resulting from dysregulated BMP signaling that leads to osteogenic differentiation of resident cells [8,42,43]. By using LDN193189 to precondition the exosomes, we effectively modulated the BMP pathway, shifting the balance toward tenogenic differentiation. This modulation of the BMP signaling pathway—a key driver of heterotopic ossification— helps to prevent aberrant bone formation within the tendon [19,44,45]. This was evidenced by reduced Runx2 expression in treated groups and the corresponding decrease in HO volume and density observed through micro-CT analysis. Our results align with earlier research indicating that BMP inhibition can substantially reduce HO formation, further supporting the potential of our dual-target strategy.

Enhancing the therapeutic efficacy of exosomes, we modified them with CBD peptides. This modification improved the localization and retention of exosomes within the 3D scaffold, leading to a more controlled and sustained release profile. Recent studies in soft and hard tissue engineering have underscored the importance of sustained exosome delivery in maintaining a localized regenerative microenvironment [46–48]. For instance, CBD-modified liposomes have been successfully used to treat spinal cord injuries in rats and reduce tendon heterotopic ossification in rodents [2,30], while CBD-modified growth factors (e.g., BMP-12, SDF-1α, FGF-18) have been applied to regenerate the enthesis and tendon–bone interfaces [5,46,49,50]. Compared to these growth factors, exosomes represent a more complex and versatile bioactive formulation. We used LDN-preconditioned exosomes to better tailor the therapeutic intervention for tendon injuries. In our study, in vitro release kinetics confirmed that CBD modification significantly prolonged exosome release, thereby ensuring a continuous supply of bioactive molecules at the injury site. This sustained release is likely a critical factor contributing to the improved ECM organization and mechanical integrity observed in the 3D-CBD@LDN/Exos group.

The structural design of the 3D scaffold also plays an essential role in tendon regeneration [51]. Constructed from PLGA and collagen I, the scaffold closely mimics the natural ECM of tendons. Its porous, loose architecture facilitates cell infiltration, nutrient exchange, and effective exosome retention. Recent advances in 3D printing technology have enabled the precise fabrication of scaffolds using materials such as collagen I and PLGA [52–54]. Collagen I, a major component of the native tendon extracellular matrix (ECM), supports cell adhesion, proliferation, and directional growth, while PLGA, an FDA-approved polymer, offers excellent mechanical strength and a controllable degradation rate. The combination of these materials allows for the creation of a biomimetic scaffold that closely replicates the native tendon microenvironment. Such scaffolds not only provide the necessary structural support but also enable a controlled and sustained release of bioactive exosomes. Our findings are consistent with recent studies exploring 3D scaffold-loaded exosome therapies in regenerative medicine. For example, sustained exosome delivery via 3D-printed scaffolds has been shown to enhance tissue repair in both bone and cartilage, primarily by preserving a microenvironment enriched with regenerative signals [24,55,56]. Similarly, in tendon repair, exosome-mediated

regulation of inflammation and ECM remodeling has been identified as a crucial factor for successful regeneration. By integrating these concepts, our study not only confirms the regenerative capabilities of tendon-derived exosomes but also introduces a novel approach that concurrently promotes tendon healing and inhibits heterotopic ossification.

While our findings demonstrate the therapeutic potential of the 3D-CBD@LDN/Exos scaffold in aged tendon repair, several translational challenges warrant consideration. Although the aged rat model provides clinically relevant insights into age-related tendinopathy, its ability to fully replicate human tendon pathophysiology remains limited, necessitating validation in larger preclinical models and eventual clinical trials. While CBD peptides exhibited low immunogenicity in rodents, their long-term safety and potential immune responses in human patients—particularly under chronic inflammatory conditions—require systematic evaluation. Furthermore, the scaffold's current degradation profile may not align with delayed healing timelines in comorbidities like diabetes, necessitating adjustable biodegradation rates. Scaling production while maintaining exosome bioactivity and scaffold consistency demands advanced quality control systems for 3D printing processes, coupled with GMP-compliant manufacturing protocols to address regulatory hurdles. Although BMP pathway modulation appears central to the observed anti-ossification effects, comprehensive multi-omics analyses are needed to fully elucidate exosome-mediated intracellular mechanisms and off-target signaling interactions. Addressing these challenges through interdisciplinary collaboration will be critical for advancing this technology toward clinical application.

5. Conclusion

In summary, our study demonstrates that a 3D scaffold loaded with LDN-preconditioned, CBD-modified exosomes can effectively promote Achilles tendon regeneration while preventing heterotopic ossification. By leveraging the synergistic effects of BMP pathway modulation and sustained exosome delivery, this dual-target strategy represents a promising new avenue for tendon repair. The integration of advanced scaffold engineering with targeted biological therapies not only improves ECM deposition and fiber organization but also restores mechanical functionality, offering significant potential for future clinical applications in the treatment of tendon injuries.

Acknowledgments and funding statement

This work was supported by the National Natural Science Foundation of China (No. 82302779), the Natural Science Foundation of Chongqing, China (CSTB2023NSCQ-BHX0218), the China Postdoctoral Science Foundation (Nos. 2024M753778 and 2023M730435), the Research Start-up Fund of Post-doctoral of SAHSYSU (Grant No. ZSQYRSFPD0057), Shenzhen Key Laboratory of Bone Tissue Repair and Translational Research (No. ZDSYS20230626091402006), and Chongqing Postdoctoral Special Funding (No. 2023CQBSHTB3102).

CRediT authorship contribution statement

Yan Xu: Writing – review & editing, Resources, Project administration, Methodology, Investigation, Funding acquisition, Data curation, Conceptualization. **Jiaqiang Huang:** Software, Methodology, Investigation, Data curation. **Yingjie Mai:** Visualization, Validation, Formal analysis. **Zhiyuan Zhang:** Visualization, Validation, Software, Project administration, Methodology. **Siqi Li:** Visualization, Software. **Haofeng Lin:** Visualization, Validation, Software, Project administration, Investigation. **Fuxin Wei:** Supervision, Resources, Project administration, Funding acquisition, Conceptualization. **Yang Chen:** Writing – review & editing, Writing – original draft, Funding acquisition, Conceptualization.

Declaration of competing interest

The authors declare that they have no known competing financial interests or personal relationships that could have appeared to influence the work reported in this paper.

Appendix A. Supplementary data

Supplementary data to this article can be found online at https://doi.org/10.1016/j.mtbio.2025.101790.

Data availability

No data was used for the research described in the article.

References

[1] N.L. Millar, G.A.C. Murrell, I.B. McInnes, Inflammatory mechanisms in tendinopathy - towards translation, Nat. Rev. Rheumatol. 13 (2017) 110–122.
[2] Y. Chen, W. Shen, C. Tang, J. Huang, C. Fan, Z. Yin, Y. Hu, W. Chen, H. Ouyang, Y. Zhou, Z. Mao, X. Chen, Targeted pathological collagen delivery of sustained-release rapamycin to prevent heterotopic ossification, Sci. Adv. 6 (2020) eaay9526.
[3] K.T. Tam, K. Baar, Using load to improve tendon/ligament tissue engineering and develop novel treatments for tendinopathy, Matrix Biology, J. Int. Soc. Mat. Biol. 135 (2025) 39–54.
[4] J.G. Lyons, F.B. Berkay, A. Minhas, Epidemiology of sports-related tendon ruptures presenting to emergency departments in the United States, Am. J. Sports Med. 52 (2024) 3396–3403.
[5] H. Xiao, Y. Chen, M. Li, Q. Shi, Y. Xu, J. Hu, X. Li, C. Chen, H. Lu, Cell-free book-shaped decellularized tendon matrix graft capable of controlled release of BMP-12 to improve tendon healing in a rat model, Am. J. Sports Med. 49 (2021) 1333–1347.
[6] M. Kjær, J. Petersen, M.R. Dünweber, J.L. Andersen, L. Engebretsen, S. P. Magnusson, Dilemma in the treatment of sports injuries in athletes: tendon overuse, muscle strain, and tendon rupture, Scand. J. Med. Sci. Sports 35 (2025) e70026.
[7] L. Fang, X. Lin, R. Xu, L. Liu, Y. Zhang, F. Tian, J.J. Li, J. Xue, Advances in the development of gradient scaffolds made of nano-micromaterials for musculoskeletal tissue regeneration, Nano-Micro Lett. 17 (2024) 75.
[8] Q. Zhang, D. Zhou, H. Wang, J. Tan, Heterotopic ossification of tendon and ligament, J. Cell Mol. Med. 24 (2020) 5428–5437.
[9] H. Feng, W. Xing, Y. Han, J. Sun, M. Kong, B. Gao, Y. Yang, Z. Yin, X. Chen, Y. Zhao, Q. Bi, W. Zou, Tendon-derived cathepsin K-expressing progenitor cells activate Hedgehog signaling to drive heterotopic ossification, J. Clin. Investig. 130 (2020) 6354–6365.
[10] C. Ouyang, T. Tu, H. Yu, L. Wang, Z. Ni, J. Yang, Y. Dong, X. Zou, W. Zhou, J. Liu, D. Chen, Y. Wang, X. Wu, H. Yi, X. Yuan, Z. Liu, H. Lu, One-step formed janus hydrogel with time-space regulating properties for suture-free and high-quality tendon healing, Adv. Sci. (2025) e2411400.
[11] H. Kürüm, H.B. Tosun, F. Aydemir, O. Ayas, K. Orhan Kürüm, F. İpekten, Surgical outcomes in patients with Achilles tendon rupture-a retrospective study, PeerJ 13 (2025) e18890.
[12] B. Walia, A.H. Huang, Tendon stem progenitor cells: understanding the biology to inform therapeutic strategies for tendon repair, J. Orthop. Res. 37 (2019) 1270–1280. Official Publication of the Orthopaedic Research Society.
[13] P.P.Y. Lui, C. Huang, X. Zhang, Selenium nanoparticles suppressed oxidative stress and promoted tenocyte marker expression in tendon-derived stem/progenitor cells, Antioxidants 13 (2024).
[14] P.P.Y. Lui, K.M. Chan, Tendon-derived stem cells (TDSCs): from basic science to potential roles in tendon pathology and tissue engineering applications, Stem. Cell. Rev. Rep. 7 (2011) 883–897.
[15] Y. Gao, H. Wang, L. Shi, P. Lu, G. Dai, M. Zhang, B. Han, M. Cao, Y. Li, Y. Rui, Erroneous differentiation of tendon stem/progenitor cells in the pathogenesis of tendinopathy: current evidence and future perspectives, Strm. Cell. Rev. Rep. 21 (2025) 423–453.
[16] Q. Yang, J. Li, H. Meng, Y. Wang, L. Hu, W. Su, J. Xu, J. Hou, R. Zhao, Z. Wang, K. Zhang, Y. Wu, L. Wang, Coaxial electrospun nanofibrous membranes as dual-functional biomimetic tendon sheath for tendon repair and anti-peritendinous adhesion, Adv. Healthcare Mater. 14 (2025) e2402074.
[17] S. Chen, Y. Lin, H. Yang, Z. Li, S. Li, D. Chen, W. Hao, S. Zhang, H. Chao, J. Zhang, J. Wang, Z. Li, X. Li, Z. Zhan, H. Liu, A CD26+ tendon stem progenitor cell population contributes to tendon repair and heterotopic ossification, Nat. Commun. 16 (2025) 749.
[18] A. Gomez-Collignon, R. Brown, A. Carr, S. Dakin, A. Lach, C. Loizou, M. Rogers, R. Sharp, A. Kendal, Single Cell Multi-Omics Characterise Discrete Human Tendon Cells Populations that Persist in Vitro and on Fibrous Scaffolds, European cells & materials, 2022, p. 44.
[19] G. Dai, Y. Li, J. Liu, C. Zhang, M. Chen, P. Lu, Y. Rui, Higher BMP expression in tendon stem/progenitor cells contributes to the increased heterotopic ossification in Achilles tendon with aging, Front. Cell Dev. Biol. 8 (2020) 570605.

[20] L. Lin, Q. Shen, T. Xue, C. Yu, Heterotopic ossification induced by Achilles tenotomy via endochondral bone formation: expression of bone and cartilage related genes, Bone 46 (2010) 425–431.
[21] Z.J. Li, Q.Q. Yang, Y.L. Zhou, Biological and mechanical factors and epigenetic regulation involved in tendon healing, Stem Cell. Int. 2023 (2023) 4387630.
[22] J. Vollaire, I. Machuca-Gayet, J. Lavaud, A. Bellanger, L. Bouazza, S. El Moghrabi, I. Treilleux, J.-L. Coll, O. Peyruchaud, V. Josserand, P.A. Cohen, The bone morphogenetic protein signaling inhibitor LDN-193189 enhances metastasis development in mice, Front. Pharmacol. 10 (2019).
[23] R.A.G. Franco, E. McKenna, P.G. Robey, M.S. Shajib, R.W. Crawford, M.R. Doran, K. Futrega, Inhibition of BMP signaling with LDN 193189 can influence bone marrow stromal cell fate but does not prevent hypertrophy during chondrogenesis, Stem Cell Rep. 17 (2022) 616–632.
[24] X. Zhang, Y. Wu, K. Han, Z. Fang, E. Cho, Y. Hu, X. Huangfu, J. Zhao, 3-Dimensional bioprinting of a tendon stem cell-derived exosomes loaded scaffold to bridge the unrepairable massive rotator cuff tear, Am. J. Sports Med. 52 (2024) 2358–2371.
[25] Y. Fan, Y. Zhou, M. Lu, H. Si, L. Li, B. Tang, Responsive Dual-Targeting Exosome as a Drug Carrier for Combination Cancer Immunotherapy, vol. 2021, Research (Wash D C), 2021 9862876.
[26] S. Bathini, D. Raju, S. Badilescu, A. Kumar, R.J. Ouellette, A. Ghosh, M. Packirisamy, Nano-Bio Interactions of Extracellular Vesicles with Gold Nanoislands for Early Cancer Diagnosis, vol. 2018, Research (Wash D C), 2018 3917986.
[27] Y. Tang, Y. Sun, J. Zeng, B. Yuan, Y. Zhao, X. Geng, L. Jia, S. Zhou, X. Chen, Exosomal miR-140-5p inhibits osteogenesis by targeting IGF1R and regulating the mTOR pathway in ossification of the posterior longitudinal ligament, J. Nanobiotechnol. 20 (2022) 452.
[28] J. Li, X. Wang, Z. Yao, F. Yuan, H. Liu, Z. Sun, Z. Yuan, G. Luo, X. Yao, H. Cui, B. Tu, Z. Sun, C. Fan, NLRP3-Dependent crosstalk between pyroptotic macrophage and senescent cell orchestrates trauma-induced heterotopic ossification during aberrant wound healing, Adv. Sci. 10 (2023) e2207383.
[29] G. Li, Q. Han, P. Lu, L. Zhang, Y. Zhang, S. Chen, P. Zhang, L. Zhang, W. Cui, H. Wang, H. Zhang, Construction of Dual-Biofunctionalized Chitosan/Collagen Scaffolds for Simultaneous Neovascularization and Nerve Regeneration, vol. 2020, Research (Wash D C), 2020 2603048.
[30] X. Liu, L. Zhang, Z. Xu, X. Xiong, Y. Yu, H. Wu, H. Qiao, J. Zhong, Z. Zhao, J. Dai, G. Suo, A functionalized collagen-I scaffold delivers microRNA 21-loaded exosomes for spinal cord injury repair, Acta Biomater. 154 (2022) 385–400.
[31] L. Zhang, C. Fan, W. Hao, Y. Zhuang, X. Liu, Y. Zhao, B. Chen, Z. Xiao, Y. Chen, J. Dai, NSCs migration promoted and drug delivered exosomes-collagen scaffold via a bio-specific peptide for one-step spinal cord injury repair, Adv. Healthcare Mater. 10 (2021) e2001896.
[32] B. Xu, Y. Wang, G. He, X. Tao, S. Gao, M. Zhou, Y. Tang, K.-L. Tang, L. Guo, W. Chen, An aligned-to-random PLGA/Col1-PLGA/nHA bilayer electrospun nanofiber membrane enhances tendon-to-bone healing in a murine model, Am. J. Sports Med. (2025) 3635465241310530.
[33] Y. Liu, L. Xu, Q. Zhang, Y. Kang, L. Liu, Z. Liu, Y. Wang, X. Jiang, Y. Shan, R. Luo, X. Cui, Y. Yang, X. Yang, X. Liu, Z. Li, Localized Myocardial Anti-inflammatory Effects of Temperature-Sensitive Budesonide Nanoparticles during Radiofrequency Catheter Ablation, vol. 2022, Research (Wash D C), 2022 9816234.
[34] C. Chen, Z.-H. Chang, B. Yao, X.-Y. Liu, X.-W. Zhang, J. Liang, J.-J. Wang, S.-Q. Bao, M.-M. Chen, P. Zhu, X.-H. Li, 3D printing of interferon γ-preconditioned NSC-derived exosomes/collagen/chitosan biological scaffolds for neurological recovery after TBI, Bioact. Mater. 39 (2024) 375–391.
[35] Ł. Pulik, B. Mierzejewski, M.A. Ciemerych, E. Brzóska, P. Łęgosz, The survey of cells responsible for heterotopic ossification development in skeletal muscles-human and mouse models, Cells 9 (2020).
[36] J. Anthonissen, C. Ossendorf, U. Ritz, A. Hofmann, P.M. Rommens, Animal models for acquired heterotopic ossification, Acta Orthop. Belg. 80 (2014).
[37] Y. He, S. Lu, W. Chen, L. Yang, F. Li, P. Zhou, Z. Chen, R. Wan, Z. Zhang, Y. Sun, J. Lin, Y. Chen, Z. Luo, C. Xu, S. Chen, Exosomes derived from tendon stem/progenitor cells enhance tendon-bone interface healing after rotator cuff repair in a rat model, Bioact. Mater. 40 (2024) 484–502.
[38] K. Song, T. Jiang, P. Pan, Y. Yao, Q. Jiang, Exosomes from tendon derived stem cells promote tendon repair through miR-144-3p-regulated tenocyte proliferation and migration, Stem Cell Res. Ther. 13 (2022) 80.
[39] M. Zhang, H. Liu, Q. Cui, P. Han, S. Yang, M. Shi, T. Zhang, Z. Zhang, Z. Li, Tendon stem cell-derived exosomes regulate inflammation and promote the high-quality healing of injured tendon, Stem Cell Res. Ther. 11 (2020) 402.
[40] J. Lu, H. Chen, K. Lyu, L. Jiang, Y. Chen, L. Long, X. Wang, H. Shi, S. Li, The functions and mechanisms of tendon stem/progenitor cells in tendon healing, Stem Cell. Int. 2023 (2023) 1258024.
[41] J.H. Boergermann, J. Kopf, P.B. Yu, P. Knaus, Dorsomorphin and LDN-193189 inhibit BMP-mediated Smad, p38 and Akt signalling in C2C12 cells, Int. J. Biochem. Cell Biol. 42 (2010) 1802–1807.
[42] Y. Xu, M. Huang, W. He, C. He, K. Chen, J. Hou, M. Huang, Y. Jiao, R. Liu, N. Zou, L. Liu, C. Li, Heterotopic ossification: clinical features, basic researches, and mechanical stimulations, Front. Cell Dev. Biol. 10 (2022) 770931.
[43] Y. Huang, X. Wang, D. Zhou, W. Zhou, F. Dai, H. Lin, Macrophages in heterotopic ossification: from mechanisms to therapy, NPJ Regen. Med. 6 (2021) 70.
[44] F. Felix-Ilemhenbhio, G.A.E. Pickering, E. Kiss-Toth, J.M. Wilkinson, Pathophysiology and emerging molecular therapeutic targets in heterotopic ossification, Int. J. Mol. Sci. 23 (2022) 6983.
[45] B. Prados, R. del Toro, D. MacGrogan, P. Gómez-Apiñániz, T. Papoutsi, P. Muñoz-Cánoves, S. Méndez-Ferrer, J.L. de la Pompa, Heterotopic ossification in mice overexpressing Bmp2 in Tie2+ lineages, Cell Death Dis. 12 (2021) 729.
[46] E. Adjei-Sowah, D.S.W. Benoit, A.E. Loiselle, Drug delivery approaches to improve tendon healing, Tissue Eng., Part B 29 (2023) 369–386.
[47] J. Cui, Y.-J. Zhang, X. Li, J.-J. Luo, L.-L. Zhao, X.-Y. Xie, W. Ding, J.-C. Luo, T.-W. Qin, Decellularized tendon scaffolds loaded with collagen targeted extracellular vesicles from tendon-derived stem cells facilitate tendon regeneration, J. Contr. Release 360 (2023) 842–857.
[48] L. Liu, W. Liu, Z. Han, Y. Shan, Y. Xie, J. Wang, H. Qi, Q. Xu, Extracellular Vesicles-in-Hydrogel (EViH) targeting pathophysiology for tissue repair, Bioact. Mater. 44 (2025) 283–318.
[49] Y. Yuan, Y. Mao, B. Sun, C. Chen, Injectable fibrocartilage-forming cores enhance bone-tendon healing in a rat rotator cuff model, Am. J. Sports Med. 53 (2025) 66–79.
[50] J. Sun, C. Mou, Q. Shi, B. Chen, X. Hou, W. Zhang, X. Li, Y. Zhuang, J. Shi, Y. Chen, J. Dai, Controlled release of collagen-binding SDF-1α from the collagen scaffold promoted tendon regeneration in a rat Achilles tendon defect model, Biomaterials 162 (2018) 22–33.
[51] C. Ning, P. Li, C. Gao, L. Fu, Z. Liao, G. Tian, H. Yin, M. Li, X. Sui, Z. Yuan, S. Liu, Q. Guo, Recent advances in tendon tissue engineering strategy, Front. Bioeng. Biotechnol. 11 (2023) 1115312.
[52] X. Yuan, W. Zhu, Z. Yang, N. He, F. Chen, X. Han, K. Zhou, Recent advances in 3D printing of smart scaffolds for bone tissue engineering and regeneration, Adv. Mater. 36 (2024) e2403641.
[53] K. Han, Y. Cheng, Q. Han, J. Chen, Extraction of type I collagen and development of collagen methacryloyl (ColMA)/PEGDA ink for digital light processing printing, Int. J. Biol. Macromol. 282 (2024) 137253.
[54] C. Wang, H. Yue, W. Huang, X. Lin, X. Xie, Z. He, X. He, S. Liu, L. Bai, B. Lu, Y. Wei, M. Wang, Cryogenic 3D printing of heterogeneous scaffolds with gradient mechanical strengths and spatial delivery of osteogenic peptide/TGF-β1 for osteochondral tissue regeneration, Biofabrication 12 (2020) 025030.
[55] Q. Li, H. Yu, F. Zhao, C. Cao, T. Wu, Y. Fan, Y. Ao, X. Hu, 3D printing of microenvironment-specific bioinspired and exosome-reinforced hydrogel scaffolds for efficient cartilage and subchondral bone regeneration, Adv. Sci. 10 (2023) e2303650.
[56] X. Sun, Y. Mao, B. Liu, K. Gu, H. Liu, W. Du, R. Li, J. Zhang, Mesenchymal stem cell-derived exosomes enhance 3D-printed scaffold functions and promote alveolar bone defect repair by enhancing angiogenesis, J. Personalized Med. 13 (2023).